ISSN 1392–1320 MATERIALS SCIENCE (MEDŽIAGOTYRA). Vol. 28, No. 3. 2022

Effects of Isocyanate-to-Polyols (NCO/OH) Ratio on Bio-based Polyurethane Film from Palm Kernel Oil based Monoester Polyols (PKO-p) for Polymer Electrolytes Application

Mohd Sukor SU'AIT [1] *, Puteri Intan Zulaikha SYED MAHADZIR [1], Khairiah Haji BADRI [2], Azizan AHMAD [2]

[1] *Solar Energy Research Institute (SERI), Universiti Kebangsaan Malaysia, 43600 Bangi, Selangor, Malaysia*
[2] *School of Chemical Sciences, AND Polymer Research Center, Faculty of Science and Technology, Universiti Kebangsaan Malaysia, 43600 Bangi, Selangor, Malaysia*

crossref http://dx.doi.org/10.5755/j02.ms.28606

Received 06 March 2021; accepted 09 September 2021

This study investigated the synthesis of bio-based polyurethane (PU) film from palm kernel oil-based polyols (PKO-p) at four different isocyanate-to-polyols (NCO/OH) ratios comprising 100/100, 100/150, 100/200, and 100/250. The PU film was prepared by mixing 2,4-methylene diphenyl diisocyanate (MDI) and PKO-p in acetone using the pre-polymerization technique under a nitrogen atmosphere at room temperature. The effect of the NCO/OH ratio on the properties of the PU films was analyzed through infra-red spectroscopy, molecular weight distribution, thermal behavior, and impedance spectroscopy. According to the infra-red spectroscopic analysis, the formation of urethane linkages (–NHCOO–) after the polymerization was indicated through the disappearance of isocyanate (N=C=O) peak and the appearances of secondary amine, carbonyl, carbamate, ether, and ester groups in the PU chain. In addition, the Gel Permeation Chromatography (GPC) showed that the weight of average molecular weight (M_W) increased with increasing NCO/OH ratio up to 1.23×10^6 g mol^{-1}. Nevertheless, higher content of PKO-p resulted in a low crosslink PU (4 % crosslink) and poor physical properties such as soft, sticky, and easy to tear due to the non-hydrogen bonded urethane. Moreover, the glass-transition temperature (T_g) reduced from 67 °C to 30 °C with the increase in PKO-p content. Despite all samples experienced the same thermal stability at 187 °C, a significant difference was observed in the mass loss of NCO/OH ratios. The highest thermal degradation was found at (100/200) NCO/OH ratio with T_{max} = 444 °C. Furthermore, the piezoelectricity characteristic of pristine PU recorded the bulk resistant of up to ~$10^7 – 10^5$ Ω which reduced further after the presence of lithium iodide (LiI) salts as the charge carrier with the calculated ionic conductivity around 10^{-5} S cm^{-1}. Thus, this study demonstrated the promising physicochemical properties of PU film from PKO-p for polymer electrolyte application.
Keywords: 2,4-methylene diphenyl diisocyanate, palm kernel oil-based monoester polyols (PKO-p), polyurethane, polymerization, polymer electrolyte.

1. INTRODUCTION

Recently, polyurethane (PU) has attracted the attention of the research community due to its wide application as a polymer electrolyte in composites [1], medical engineering [2], coatings and adhesives, and electrochemical devices [3 – 6]. In particular, the physical stability and flexibility to withstand the pressure between the anode and cathode are essential characteristics of polymer electrolytes to function properly in electrochemical devices. These characteristics depend on the chemical structure of the polymer electrolyte's backbone which consists of soft and hard segments [7]. The former can adjust the flexibility and elasticity while the later enhances the strength and rigidity through crosslinking process [7, 8].

According to Filip and co-workers, the soft segment enhances the stronger ionic interactions and solvation capacity of ions, consequently contributing to the higher ionic conductivity [9]. This unique characteristic could be achieved by controlling the mole ratio of the hard segments to soft segments (isocyanates-to-polyols NCO/OH) in PU. Nonetheless, diisocyanate with two or more functional groups is required to form the hard segment in PU. Apart from being less reactive than the aromatic group, aliphatic isocyanates are only used in the final product, which requires specific properties, such as light stable coatings and elastomeric functionality. Even within the same class of isocyanates, there are significant differences in the reactivity of the functional groups due to the steric hindrance. Methylene diphenyl diisocyanate (MDI) itself has three isomers comprising 4,4'-MDI, 2,4'-MDI, and 2,2'-MDI. In the case of 2,4'-MDI, the isocyanate group in the para position to the methyl group is much more reactive than the isocyanate group in the ortho position [10].

Conventional polyester polyols are commonly used to form the selection of the soft segments by direct poly-esterification of high-purity diacids and glycols. They are distinguished by the choice of monomers, molecular weight, and the degree of branching. In addition, they offer desirable physical properties such as superior solvent, abrasion, and low resistance that could not be obtained in petrochemical-based polyether polyols, for instance, polyethylene glycols (PEG).

* Corresponding author. Tel.: +603-89118575; fax: (60)389118574.
E-mail address: *mohdsukor@ukm.edu.my* (M.S. Su'ait)

In contrast, bio-based polyester polyols are derived from vegetable oils which provide better elastomeric properties, are flexible, and are easy to be molded to serve as the potential biomaterial for soft tissue engineering applications [11] and elastomeric application [12]. Palm kernel oil-based polyols (PKO-p) are derived from vegetable oils that possess a high content of saturated fats of lauric acid (45 ~ 54 %), which is more saturated than palm oil and comparable to coconut oil [13 – 15]. In the last decade, synthesized PKO-p has been found to possess lower glass-transition temperature (T_g) compared to soy oil-based polyols after the polymerization reaction [16]. The low T_g value implies greater segmental motion of its polymeric chain, thus is favorable for the development of polymeric electrolytes with high conductivity [17, 18].

Furthermore, research on PKO-p has been extensively studied by Badri and her research groups [5, 19 – 25] as the choice of monomers at laboratory scale as well as in pilot scale system for various applications including composites, castable elastomer, rigid and flexible foams, adhesives and coatings in order to accommodate the demand required for commercialization [26].

In this study, PU film was synthesized from PKO-p at different (NCO/OH) weight percent ratio (wt.%) via pre-polymerization reaction, and the physicochemical properties of the bio-based PU film was characterized through infra-red spectroscopy, molecular weight distribution, thermal behavior analysis, and impedance spectroscopy. It was expected that the synthesis of PU at different weight percentages of NCO/OH would result in significant physical and electrochemical properties of the desired PU films. The novelty of this study was motivated by the synthesis of bio-based PU film as alternative sources for various applications including biopolymer host electrolytes.

2. EXPERIMENTAL

2.1. Materials

An industrial-grade 2,4′- diphenylmethane diisocyanate (2,4-MDI) pure monomeric (99.8 %) was purchased from Behn Meyer Chemicals (M) Sdn. Bhd, Subang Jaya, Selangor, Malaysia; Palm kernel oil-based polyols (PKO-p) was prepared as described in several established method by [4, 5, 14, 27 – 29]. Acetone (CAS. No: 67-64-1) was supplied by Systerm ChemAR, Poland. All chemicals were used without further purification.

2.2. Sample preparation

PKO-p was mixed with 2,4-MDI in acetone at different NCO/OH weight percent ratios (wt.%) of 100/100, 100/150, 100/200, and 100/250. Table 1 summarizes the chemical composition at different NCO/OH ratios and its conversion from weight ratio to molar ratio. The procedure was conducted at room temperature under a nitrogen gas atmosphere. The solution was stirred to form a homogenous solution for five minutes. Then, the solution was cast onto a Teflon mold and allowed to evaporate at room temperature for an hour. The synthesis was carried out at room temperature without the presence of catalysts, surfactants, additives, crosslinkers, or chain extenders. The presence of an amine functional group in PKO-OH provided an alternative route for catalyzing PU polymerization [25]. Once the produced film was formed, the characterization of the samples was performed.

2.3. Characterization of synthesized PU film

2.3.1. Infra-red spectroscopy

The attenuated total reflectance – Fourier transform infrared spectroscopy (ATR-FTIR) was performed to observe the formation of the urethane backbone (–NHCOO–). ATR-FTIR spectra were recorded measured by a computer interfaced with Spectrum 400 Perkin Elmer GX spectrometer. The PU films were placed onto the ATR crystal and analyzed in the frequency range of 4000 cm^{-1} to 650 cm^{-1} at a scanning resolution of 2 cm^{-1}.

2.3.2. Molecular weight distribution

The gel permeation chromatography (GPC) was carried out to determine the weight average molecular weight (M_w) and the number average molecular weight (M_n) of the PU film. The M_w describes the average weight of molecular mass in each component, while the M_n denotes the average molecular weight of all individual molecules divided by the total number of molecules [30]. Given that polymer molecules, even the same type, come in different sizes (chain lengths for linear polymers), an average value would be suitable to represent the approximate size of the entire structure. The homogenous dispersion of distribution is denoted by dispersity ($Đ$), which corresponds to the measurement of the dispersion of macromolecule in the polymeric sample [31].

Table 1. Conversion from weight ratio molar ratio at different NCO/OH ratios

Weight ratio, NCO/OH	Molar ratio, NCO/OH
100/100	2/2.4
100/150	2/3.6
100/200	2/4.9
100/250	2/6.1

The gel content measurement was performed by using the Soxhlet extraction technique with toluene as a solvent for 24 hours. The residue was then dried and weighed until a constant weight was achieved. The percentages of sol and gels were calculated to determine the percentage of crosslink in the PU network by [32]:

$$\text{Sol content (SC\%)} = (W_1 - W_2/W_1) \times 100\% \quad (1)$$

$$\text{Gel content (GC\%)} = 100 - (\text{SC\%}) \quad (2)$$

where W_1 is the mass of the sample before extraction, g; W_2 is the mass of the sample after extraction, g.

The analysis was carried out in a Polymer Laboratories model PL-GPC 50 plus using Styragel HR 5 tetrahydrofuran (THF) column coupled with WATERS 2414 reflective index detector at 40 °C with 1 mL/min flow rate of (THF; 99.9%, Merck). The setup was standardized by using polystyrene standards. Approximately 0.03 g of sample was weighed and solubilized in 10 mL of THF for 24 hours before the measurement was performed.

2.3.3. Thermal behavior analysis

Differential scanning calorimetry (DSC) is a useful method to determine the thermal properties of polymers. The (T_g) of the samples were observed using Mettler-Toledo DSC model 822e from 20 to 250 °C at a scanning rate of 10 °C/min under a nitrogen gas atmosphere. Approximately, 4 mg of PU film was used for each DSC measurement. The T_g of the PU films at the mid-point of the endothermic peak was evaluated from the STARe software.

In addition, thermogravimetric analysis was carried out to characterize the thermal properties of the PU films. A Mettler-Toledo TGA/simultaneous difference thermal analysis (SDTA) 851 instrument was equipped under a nitrogen gas atmosphere from room temperature to 600 °C at a heating rate of 10 °C/min. Approximately 5 mg of sample in the form of fine powder was used to determine the weight loss of the polymers.

2.3.4. Impedance spectroscopy

The electrochemical impedance spectroscopy (EIS) was utilized to evaluate the resistivity level of the PU films. A high frequency resonance analyzer (HFRA) model 1255 was used with the applied frequency from 1 MHz to 0.1 Hz at 1000 mV amplitude. The resistivity and the ionic conductivity were obtained by the equations:

$$\rho = (A \cdot R_b)/l; \quad (3)$$

$$\sigma = 1/\rho, \quad (4)$$

where A is the contact area of the sample, R_b is the electrical resistance of a uniform sample of the material and l is the length of the sample. The bulk resistance (R_b) was determined from the equivalent circuit analysis using the Z_{view} analyzer software, in which the contact area of the thin film (A = 2.01 cm^2), and average thickness was measured using a Mitutoyo digital caliper was 0.01 cm [33].

Impedance is a complex quantity comprised of two parts: the real part, Z_r and the imaginary part, Z_i. The contributions to Z_i involve the quantity j where j = –1. Both Z_r and Z_i are related to Z as expressed in the following equation:

$$Z = Z_r - jZ_i, \quad (5)$$

where Z_r and Z_i can be displayed as a complex plane (also known as Nyquist Plot) in which Z_i (y-axis) is plotted against Z_r (x-axis) [34].

3. RESULTS AND DISCUSSION

3.1. FTIR analysis

The molecular structure of MDI and the progress of the reaction between PKO-p and MDI to form PU were estimated from the FTIR spectra as shown in Fig. 1. Based on Fig. 1 a, a significant strong peak at 2241 cm^{-1} corresponded to the isocyanate (N=C=O) of pure 2,4-MDI. Upon reaction with PKO-p at 100/100 NCO/OH ratio, traces of N=C=O in the vibrational region of 2276 cm^{-1} were observed. This signifies that the polymerization reaction at 100/100 ratio (equivalent to NCO/OH molar ratio of 2:2.43) led to the termination of pre-polymer urethane due to the low amount of excess isocyanate reagent that leads to incomplete reaction.

Theoretically, 2 mol of MDI is required to react with 3 mol of PKO-OH from the reaction scheme to completely polymerize PU based PKO-p. The mechanism was proven by the disappearance of the N=C=O peak indicating that the isocyanate completely reacted with the monoester polyols from PKO-p to form polyurethane with the increase in NCO/OH ratio starting from 100/150. The complete PU polymerization reaction, which involved the additional polymerization via step-growth polymerization reaction between MDI and excess PKO-p [35].

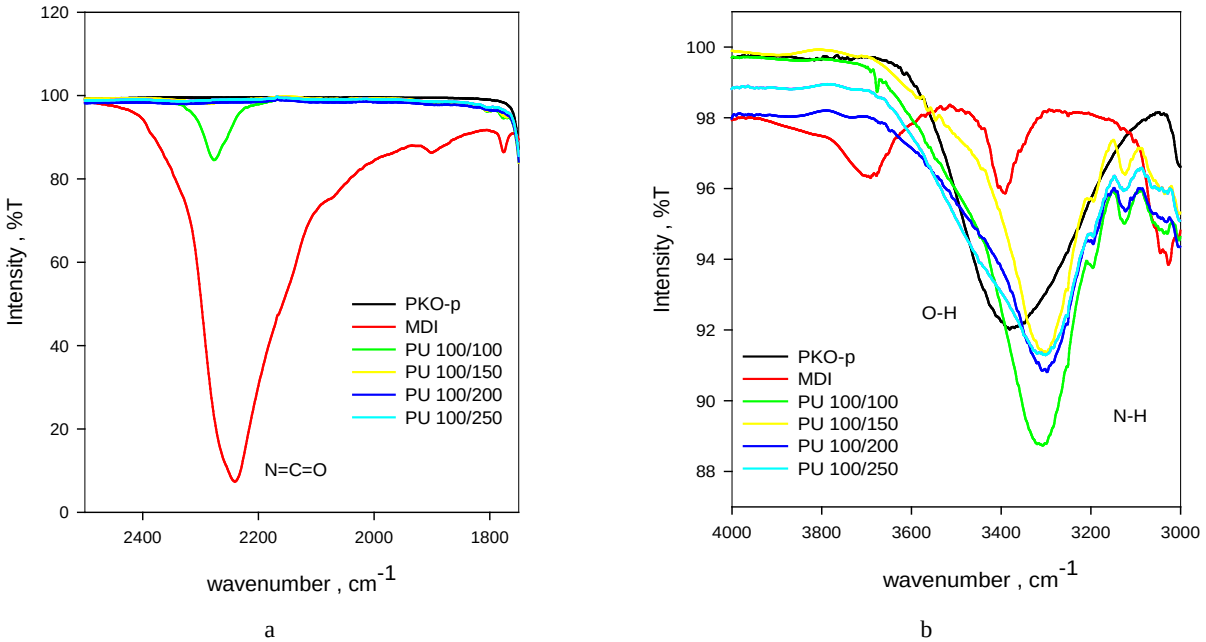

Fig. 1. a – FTIR spectra of ν(N=C=O) functional groups PU; b – FTIR spectra of (O–H) and (N–H) stretching functional groups in PU

Fig. 1 b illustrates the vibrational region between 3000 cm^{-1} to 4000 cm^{-1}. In this study, the (O–H) functional group was found at 3381 cm^{-1} in PKO-p synthesized from palm kernel oil by using esterification technique developed by Badri et al. [25]. The presence of an O–H vibrational peak was believed might be due to the moisture (H_2O) produced during the esterification process. The water content was approximately ± 0.2 % as given by Karl Fischer titration analysis. After polymerization, a single band of N–H peaks which belongs to the stretching mode of hydrogen bonded N–H with oxygen (ether) appeared at 3307 cm^{-1}, 3298 cm^{-1}, 3297 cm^{-1}, and 3300 cm^{-1} for 100/100, 100/150, 100/200 and 100/250 ratio respectively [35, 36].

The occurrence of a single band of N–H peaks after the polymerization indicated the presence of secondary amides (–NHCO–) in the polymeric structure. The secondary amides mainly existed in the *trans*-conformation due to the free N–H stretching vibration near 3430 cm^{-1}. This peak will shift to the vibrational region between 3320 – 3140 cm^{-1} due to the formation of new hydrogen bonding in the free N–H band. However, tertiary amides in PKO-p did does not show any absorption band in this region.

Fig. 2 a shows the vibrational region of carbonyl (C=O), carbamate (C–N) and N–H.

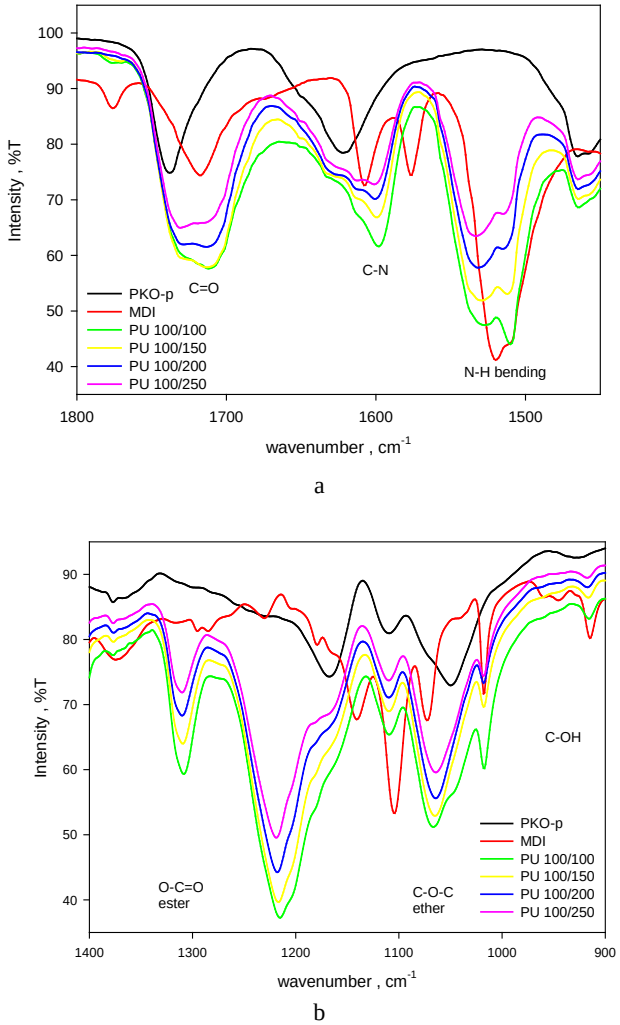

Fig. 2. a – FTIR spectra of v(C=O), v(C–N) and (N–H) bending functional groups PU; b – FTIR spectra of v(C–O–C) and v(O–C=O) functional groups in PU

The functional group of C=O for polyols PKO-p was observed at 1738 cm^{-1}. However, the C=O frequency of tertiary amides was independent of its physical state as it was not possible to form hydrogen bonding with another tertiary amide group [37]. Furthermore, the C=O functional group for isocyanate in MDI was found at 1717 cm^{-1}. After polymerization, the C=O group for PU was observed at 1712 cm^{-1}, 1713 cm^{-1}, and 1713 cm^{-1} for 100/100, 100/150 and 100/20 ratios respectively. In contrast, it was believed that the C=O functional group at 1713 cm^{-1} 100/250 ratio was affected by the non-hydrogen bonded urethane stretching.

According to previous studies [38,39], the existence of the peak at ~1740 cm^{-1} was associated with the non-hydrogen bonded urethane stretching while the peak around ~1700 cm^{-1} was assigned to hydrogen-bonded urethane stretching. This indicates that the existence of intermolecular interaction in this pre-polymerization technique due to the lower frequencies of C=O absorption.

In addition, this low-frequency absorption is also due to the resonance structure in the amide functional group as shown in Fig. 3. The resonance structure of amide functional groups was found at 1598 cm^{-1}, 1599 cm^{-1}, 1601 cm^{-1}, and 1601 cm^{-1} for 100/100, 100/150, 100/200, and 100/250 ratio respectively. All vibrational regions were approximately at 1600 cm^{-1}, which corresponded to C–N groups. In secondary amides, the C–N stretching vibration was observed to have a similar frequency with the N–H bending mode. The interaction (coupling) of these two vibrations in the C–N–H component gives rise to N–H bending at a higher frequency (1550 – 1510 cm^{-1}). The intensity of N–H bending found at 1510 cm^{-1} is reduced and shifted to 1515 cm^{-1} with the increasing of NCO/OH ratio. In comparison, the intensity of neighboring peaks at 1528 cm^{-1} increased and shifted to 1533 cm^{-1}. The peak at 1050 cm^{-1} in Fig. 2 b was assigned to C–OH group of PKO-p.

After polymerization, this peak was observed at ~1065 cm^{-1} which belongs to the ester (C–O–C) functional groups. The appearance of two strong peaks for O–C=O at ~1217 cm^{-1} and ~1309 cm^{-1} after polymerization indicated the formation of the urethane linkages. In contrast, the stretching mode of $–CH_2$ and $–CH_3$ peaks for all samples were found at ~2922 cm^{-1} and ~2852 cm^{-1}. Therefore, the disappearance of N=C=O peaks at ~2241 cm^{-1} and the appearances of N–H, C=O, C–N and C–O–C at ~3300 cm^{-1}, 1713 cm^{-1}, ~1600 cm^{-1}, and ~1065 cm^{-1} respectively, as well as O–C=O peaks at ~1217 cm^{-1} and ~1309 cm^{-1} after the polymerization proved that the urethane linkages were formed.

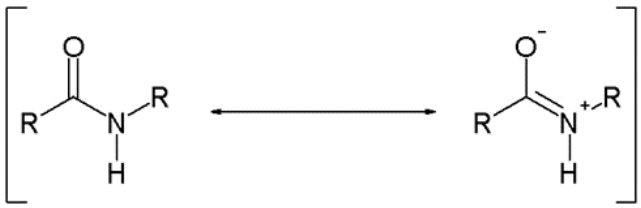

Fig. 3. The resonance structure of amide functional groups [37]

3.2. Degree of crosslinking

Table 2 shows the percentage of sol (% sol) and gel content (% gel) for PU prepared at different NCO/OH ratios. Higher content of PKO-p at 100/250 ratio produced alow crosslink PU of 4 %. The low crosslink PU was affected by the non-hydrogen bonded of urethane linkages as observed in the FTIR section and reflected the low physicals interaction between the polymeric segments. This contributed to the lack of physical properties such as soft, sticky, and easy to tear. In contrast, the low content of PKO-p at 100/100 produced a higher degree of crosslinking 85 % with better characteristics like hard, stiff, and brittle film. The high degree of physical crosslink was a result of the hydrogen bonding occurring at urethane pre-polymer as proven by the FTIR analysis. Based on the results, the PU at ratios of 100/150 and 100/200 provided flexible film, which was preferable to be applied in a wide range of solid-state device applications.

Table 2. Percentage of sol (% sol) and gel content (% gel) at different NCO/OH ratios

Sample, NCO/OH	% sol	% gel
PU 100/100	15	85
PU 100/150	27	73
PU 100/200	53	47
PU 100/250	96	4

3.3. Weight average molecular weight (M_w), number average molecular weight (M_n), and dispersity ($Đ$)

Table 3 shows weight average molecular weight (M_w), number average molecular weight (M_n), and dispersity ($Đ$), derived from gel permeation chromatography (GPC) analysis. The calculated M_w for the well-established monoester PKO-p sample was ~300 g mol^{-1}. According to the GPC analysis, the M_w for 100/100 NCO/OH ratio was calculated around 3.96×10^4 g mol^{-1} in which the trend increased with the increase of polyols content up to 1.22×10^6 g mol^{-1} at 100/250 ratio. The higher M_w value for the 100/250 ratio was affected by the non-hydrogen bonded urethane linkages as observed in the FTIR studies, which contributed to a low degree of crosslinking. The dispersity for the entire ratio is greater than 1 because M_w for each ratio is greater than M_n. The wide range of molecular mass is called polydispersed polymers.

Table 3. Weight average molecular weight (M_w), number average molecular weight (M_n), and dispersity ($Đ$) of PU at different NCO/OH ratios

Sample	Molecular weight M_w, g mol^{-1}	Molecular number M_n, g mol^{-1}	Dispersity M_w/M_n
PU 100/100	3.96×10^4	2.60×10^4	1.52
PU 100/150	1.64×10^5	8.19×10^4	2.00
PU 100/200	1.71×10^5	6.50×10^4	2.63
PU 100/250	1.23×10^6	6.83×10^5	1.80

The dispersity values increased with the increase of polyols content up to 100/200 ratio and decreased at 100/250 ratio. In addition, the 100/200 ratio was observed to exhibit the highest polydispersed polymers in the polymeric structure with dispersity = 2.63 followed by 100/150, 100/250, and 100/100 ratios at 2.00, 1.80 and 1.52, respectively.

3.4. Thermal studies

DSC is capable of demonstrating improvements in heat power or latent heat, as well as tolerating melting and crystallization temperatures. DSC thermogram results for all samples prepared of PU films at various NCO/OH ratio are shown in Fig. 4 a. The T_g of PU film was examined at 67, 61, 54, and 30 °C for 100/100, 100/150 and, 100/200 and 100/250 NCO/OH ratios, respectively. The T_g value was reduced with the increase of PKO-p soft segment content, which was attributed to the hydrogen bonding formed between the PU. The decline of T_g was also correlated with the increase in the molecular weight of PU. Previous studies have suggested that the T_g value decreased as its chain length increased [38]. The same literature also reported that the decrease of T_g was related to the larger mobility of the PU macromolecule, which was based on two mechanisms. The first mechanism involved separating the hard and soft segments led to greater flexibility of the soft segments and larger molecular mobility of the polyol chains. The second mechanism occurred for all polymers and was based on the changes of the main PU chain, which resulted in higher vibration and mobility of the macromolecular structure.

It is well understood that the high degree of crosslinking required a greater amount of thermal energy and space for the polymeric chain to initiate the movements. As a consequence, a high T_g value was observed for polymeric macromolecules [11, 39]. This corresponded to the findings on the % sol and % gel as discussed earlier.

In addition, the higher degree of physical crosslinking (85 %) in the prepared PU with 100/100 NCO/OH ratio recorded the highest T_g value at 67 °C, which was characterized by the hard, stiff, and brittle texture of the film. The results indicated that the samples with the highest hard segments content possessed less miscibility between the hard and soft segments due to the tendency to interact with each other. Thus, they became less hindered as they were less dispersed in the soft segments, allowing the higher degree of phase separation in the PU structure [40]. Based on the DSC thermogram for the 100/150 ratio sample, a small crystallization temperature (T_c) of the soft segments (exothermic peak) appeared at 148 °C, while a corresponding melting temperature (T_m) of the crystalline fraction of soft segments appeared at 160 °C. However, these peaks were too small to be accounted for as T_c and T_m. Interestingly, other ratio samples did not show any obvious crystallization and melting peaks in the thermogram. The absence of these peaks indicated that the PU exhibited thermosetting properties.

Moreover, the TGA results showed that the oxidation and decomposition took place after 200 °C in all NCO/OH ratios. Since the decomposition and oxidation reactions produced weight changes in the polymeric materials, the results indicated the stability of the samples at high temperature. Polymer electrolytes must generally be thermally stable to ensure system efficiency and safety even at high temperatures [17]. Furthermore, Fig. 4 b shows the TGA thermogram and differential thermogravimetric (DTG) curves for PU films at various NCO/OH ratios.

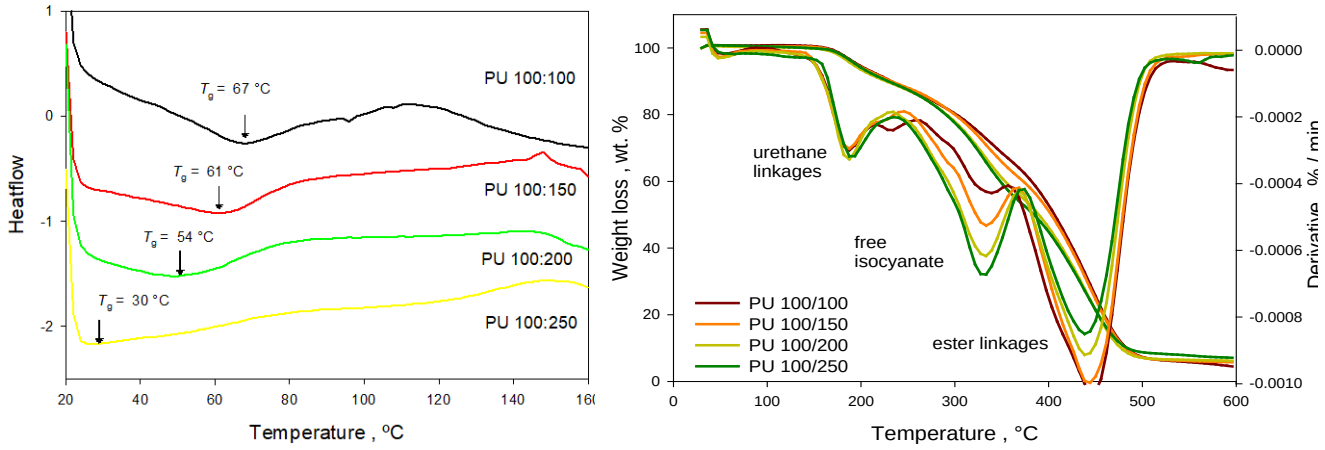

a b

Fig. 4. a – DSC thermogram of PU films at various NCO/OH ratios; b – TGA thermogram and DTG curves of (i) MDI, PKO-p and (ii) PU films at various NCO/OH ratios

Table 4. Percentage of weight loss (wt.%) at different NCO/OH ratios

Sample, NCO/OH	Weight loss, wt.%			Total weight loss, wt.%	Residue after 600°C, %
	T_{d1}, 150 – 220°C	T_{d2}, 240 – 370°C	T_{d3}, 370 – 520°C		
PU 100/100	14	20	62	96	4
PU 100/150	12	27	55	94	6
PU 100/200	11	33	50	94	6
PU 100/250	11	36	46	93	7

The wt.% is also listed in Table 4. Thermal degradation of 2,4-MDI ($T_{d\ MDI}$) was observed at 240 °C, while the maximum (T_{max}) was at 302 °C. In contrast, the thermal degradation for PKO-p ($T_{d\ PKO\text{-}p}$) was found at 320 °C with the T_{max} at 367 °C.

In general, the slight weight loss (Fig. 4 b) in the 20 – 100 °C region was related to the vaporization of moisture and solvent's residue. After polymerization, the first degradation stage of PU was observed at the 150 – 220 °C region with a thermal stability range was between 155 – 160 °C with the T_{max}, 187 °C for all NCO/OH ratios. The T_{d1} corresponded to the degradation of the hard segmented copolymer block of the urethane linkages that resulted in three stages mechanisms for the decomposition of urethane bonds: (i) the dissociation to isocyanate and alcohol, (ii) the formation of primary amine, carbon dioxide and (iii) the formation of a secondary amine and carbon dioxide [17, 40 – 42].

The second degradation stage T_{d2} for 100/100 ratio recorded almost 20 % weight loss with T_{max} at 339 °C, which increased to 36 wt.% for 100/250 ratio with T_{max} at 333 °C. This region corresponded to the liberation of free isocyanate, which led to the formation of thermally stable carbodiimide derivatives or compounds with isocyanurate rings as a result of a trimerization reaction [43]. The third degradation stage (T_{d3}) began in the 370 – 520 °C region, which was contributed by the thermal decomposition of soft segments of PU (ester linkages) and was rarely affected by the chemical composition and the three-dimensional arrangement of PU structure [38, 42]. It was revealed that almost 62 % of weight loss was observed at 100/100 ratio and only 55 wt.% for 100/150 ratio at the similar T_{max} = 438 °C. The weight loss was further reduced to 50 wt.% for 100/200 ratio and 46 wt.% for 100/250 ratio with a higher T_{max} = 444 °C.

A significant difference was observed during the degradation stage around 400 °C for all cases, which was probably resulted from the molecular weight, or the particle size [44]. The thermal stability at T_{max} of 444 °C of 100/200 ratio at T_{d3} was found to be higher than those of 100/150 (T_{max} = 438 °C), although T_{d1}, T_{d2}, T_{d3} and residue were equivalent to both ratios [45].

3.4. Impedance spectroscopy studies

The impedance plots of pure PU films at various NCO/OH ratios are shown in Fig. 5, while the equivalent circuit models, bulk resistance, and resistivity of pristine PU films for respective NCO/OH ratios are provided in Table 5. Fig. 5 a demonstrated a straight line on an imaginary plane. This characteristic resembles a pure capacitor (C_1) characteristic, which was only contributed by the imaginary part of the impedance plot. The capacitor's impedance characteristics decrease as the frequency is raised.

In contrast, the complex impedance plots of PU at 100/100 NCO/OH ratio displayed an equivalent circuit model of a series of resistance (R_1) and capacitance (C_1) which correspond to perfect model for a metal with an undamaged high impedance coating. The intercept of the curve with the real axis estimated of the surface resistance (R_1) between electrode and polymeric membrane, 19 Ω could be ignored. The presence of capacitance element parallel to the imaginary axis indicates a capacitive behavior (straight line) of the PU coating [36].

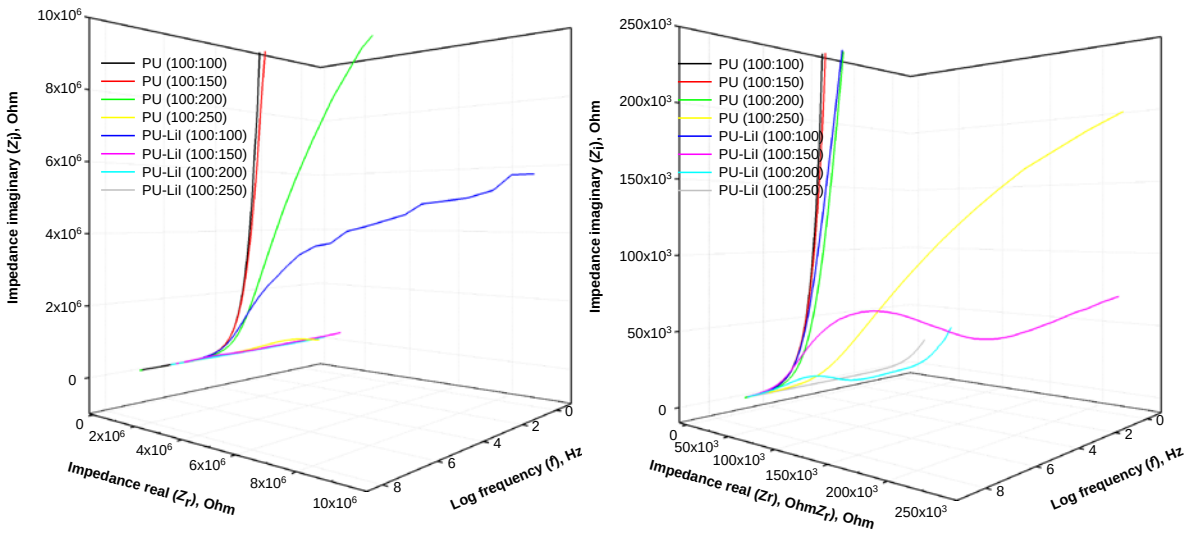

Fig. 5. Impedance plots: a – PU films and PU-LiI (25 wt.%) polymer electrolyte at various NCO/OH ratios; b – is an enlarged impedance plot

Table 5. Electrical properties of pristine PU and PU-LiI (25 wt.%) polymer electrolyte films at different NCO/OH ratios

Pristine PU					
Sample	Equivalent circuit	Capacitance, F	Bulk resistance, Ω	Resistivity, Ω cm	Dielectric strength, ε_r
PU 100/100	R_1 C_1	7.83×10^{-11}	–	–	–
PU 100/150	R_1 C_1	7.46×10^{-11}	–	–	–
PU 100/200	C_1 R_1 CPE_1	9.46×10^{-11}	5.91×10^{7}	1.19×10^{10}	0.01
PU 100/250	C_1 R_1	1.15×10^{-10}	7.92×10^{5}	1.59×10^{8}	0.01
PU-LiI (25 wt.%)					
Sample	Equivalent circuit	Capacitance, F	Bulk resistance, Ω	Conductivity, S cm^{-1}	Dielectric strength, ε_r
PU 100/100	C_1 R_1 W_1	1.14×10^{-10}	9.92×10^{6}	5.44×10^{-10}	0.01
PU 100/150	C_1 R_1 W_1	5.10×10^{-11}	1.66×10^{5}	6.13×10^{-8}	0.01
PU 100/200	C_1 R_1 W_1	7.74×10^{-11}	2.29×10^{4}	6.42×10^{-7}	0.03
PU 100/250	C_1 R_1 W_1	1.13×10^{-9}	1.97×10^{2}	5.33×10^{-5}	0.20

A capacitor is formed when two conducting plates are separated by a non-conducting media, called the dielectric. The behavior of dielectrics materials under the application of alternating voltage is mainly dependent on the contacts between the metal electrodes and the dielectric material. Therefore, with blocking electrodes, the observed transient current was contributed by the polarization of the material, which may be due to either the orientation of electric dipoles or by the hopping of positive and/or negative charges [44 – 47].

However, the value of the capacitance cannot be determined from the impedance plot. It can be determined by a curve fit or from an examination of the data points. The value of the capacitance depends on the size of the plates, the distance between the plates and the properties of the dielectric, which is expressed in the following relationship:

$$C = \frac{\varepsilon_0 \varepsilon_r A}{d}, \quad (6)$$

where; ε_o is the electrical permittivity ε_r is the relative electrical permittivity ($\varepsilon_r = 4-8$ for organic coating), A is the surface area of one plate and d is the distances between two plates.

The complex impedance plots of PU at 100/200 NCO/OH ratio in Fig. 5 b consisted of an equivalent circuit model contain parallel capacitance (C_1), resistance (R_1), and constant phase element (CPE). The PU film with 100/200 ratio recorded the bulk resistant value of 5.91×10^7 Ω, the resistivity of 1.19×10^{10} Ω cm and the calculated conductivity of 8.42×10^{-10} S cm^{-1}. A good polymeric coating is indicated by the formation of a barrier that allows a very limited current flow. On the other hand, a heavy current flow indicates a poor barrier where the moisture could permeate the coating and set up conditions for corrosion. Furthermore, the presence of the CPE element represents the homogeneity on the electrode surface because electrical double layer. This behavior may be regarded as non-ideal capacitors defined by the constants Y and n, and their impedance is given according to the equation [48]:

$$Y_{CPE} = Y_0 \, w^n \{\cos(n \, p/2) + j \sin(n \, p/2)\} \quad (7)$$

where if $n = 1$ the CPE represents an ideal capacitor $C = Y_0$; if $n = 0$ the CPE represents a resistor $R = 1/Y_0$; if $n = -1$, the CPE represents an inductor $L = 1/Y_0$; if $n = 0.5$ the CPE represents a Warburg element $W = Y_0$.

The complex impedance plots of PU at 100/250 NCO/OH ratios in Fig. 5 a exhibited a sinusoidal impedance curve, depressed, flattened semicircles in the high frequency range that is related to the conduction process in the bulk of complex [34, 45, 49]. The plot indicated the simplest and most common cell models, known as the Randles cell. The plot for the Randles cell is designated with the identical equivalent circuit model contain parallel capacitance (C_1) and R_1 as a function of capacitive current and charge–transfer resistance [50]. The PU film with 100/250 recorded a bulk resistant value of 7.92×10^5 Ω and the calculated resistivity of 1.59×10^8 Ω cm. The conductivity values were contributed by the dielectric behaviors of the polymeric membrane. According to Skoog and Holler (2007), a dielectric sub-class, piezoelectricity is defined as the electric charge that accumulates in certain solid materials, such as crystals, ceramics, and biological matters in response to the applied mechanical stress as a result of mechanical pressure [51].

In terms of the polymeric membrane, the polarity of intertwined long-chain molecules attracts and repels each other when an electric field was applied. Therefore, the observed transient current was due to the polarization of the material [52]. The conductivity value was found to increase with the addition of PKO-p content due to the soft segment PU contributed by PKO-p that acts as plasticizer. In addition, the soft segment PU could act as polymeric solvent to solvate the cations [7].

Fig. 5 b illustrates the complex impedance plot of PU films with the addition of 25 wt.% of LiI salts as charge carrier, while Table 5 presents the fitted curves modeled by the equivalent circuit analysis. The fitted curves extended the Randles cell with the addition of Warburg impedance (W) into an equivalent circuit model. Warburg impedance is a type of resistance to mass transfer in which a faradaic process could not be represented by simple linear circuit elements such as R or C, whose values are independent of frequency. The simplest representation was obtained by applying the faradaic impedance as a series combination comprising the series resistance (R_s) and the pseudocapacity (C_s) to Warburg impedance (W). The measured bulk resistance was 9.92×10^6 Ω with an ionic conductivity of 5.44×10^{-10} S cm^{-1} for pre-polymer PU at 100/100 ratio. The increase of PKO-p content in PU 100/150 ratio decreased the bulk resistance's magnitude by one order and raised the ionic conductivity to 6.13×10^{-8} S cm^{-1}.

In addition, the bulk resistance value for the PU film with 100/200 ratio was further reduced to 2.29×10^4 Ω and the ionic conductivity to 6.42×10^{-7} S cm^{-1}. In contrast, the PU film with a 100/250 ratio provided the lowest bulk resistance of 1.97×10^2 Ω with the highest calculated ionic conductivity of 5.33×10^{-5} S cm^{-1}. The values achieved were comparable to the previous report on plasticized PU with ethylene carbonate (EC) [53]. The presence of plasticizers such as polypropylene carbonate (PC) and EC in the polymer electrolyte could easily corrode in the lithium metal electrode in the electrochemical cell [45, 54].

4. CONCLUSIONS

This study revealed that all the bio-based polyurethane (PU) compounds were successfully synthesized from PKO-p at different NCO/OH ratios using the pre-polymerization technique. The 100/200 NCO/OH ratio showed promising characteristics with higher thermal stability (T_{max} = 444 °C) and higher dispersity ($Đ$) value in which the former was associated with high a flashing point that improved the safety of energy storage devices. The 100/200 ratio also exhibited a moderate average weight molecular weight (M_w) of ~1.23×10^6 g·mol^{-1}, glass transition temperature (T_g) value at 54 °C, and degree of crosslinking of 47 %. In contrast, the 100/250 NCO/OH ratio demonstrated the highest calculated ionic conductivity at ~5.33×10^{-5} S cm^{-1} with the lowest bulk resistance of 1.97×10^2 Ω in the presence of LiI. In short, the successful formation of PU films with favorable physicochemical properties, such as homogenous surface, free-standing, flat, flexible, and suitable elasticity indicated a promising biopolymer

electrolyte host that could serve as an alternative source for various purposes, including polymer electrolyte application.

Acknowledgments

The authors would like to extend their gratitude to the Universiti Kebangsaan Malaysia for allowing this research to be carried out. We would also like to extend our appreciation to Prof. Dr. Rusli Daik for assisting the TGA services. Last but not least, we would like to acknowledge all of the supports that have been given throughout the preparation of this manuscript. This work is supported by the DIP Grant UKM (DIP-2018-008), and Fundamental Research Grant Scheme, FRGS/1/2011/TK/UKM/02/39.

REFERENCES

1. **Yu, T., Jiang, F., Cui, X., Cao, M., Guo, C., Wang, Z., Chang, Y.** Properties and Mechanism of a Novel Metallic-Hollow-Spheres/Polyurethane Acoustic Composite *Journal Applied Polymer Science* 138 (8) 2021: pp. 1 – 10. https://doi.org/10.1002/app.49891
2. **Zhang, Y., Li, T.T., Shiu, B.C., Sun, F., Ren, H.T., Zhang, X., Lou, B.W., Lin, J.H.** Eco-Friendly Versatile Protective Polyurethane/Triclosan Coated Polylactic Acid Nonwovens for Medical Covers Application *Journal of Cleaner Production* 282 2021: pp. 124455. https://doi.org/10.1016/j.jclepro.2020.124455
3. **Su'ait, M.S., Jumaah, F.N., Faizzi, H.M., Mamat, S., Ludin, N.A., Farhan, W.A., Haron, A., Atifah, N., Latif, M.N., Badri, K.H., Ahmad, A.** Palm-Based Polyurethane-Ionic Liquid Gel Polymer Electrolyte for Quasi-Solid State Dye Sensitized Solar Cell *Industrial Crops and Products* 113 2018: pp. 406 – 413. http://dx.doi.org/10.1016/j.indcrop.2018.01.008
4. **Faizzi, M., Ahmad Ludin, N., Su'ait, M.S., Mohamed, N.M., Sahudin, M.A., Badri, K.H., Ahmad, A.** Effects of Iodide/Triiodide (I^-/I_3^-) Ratios on Palm Based Polyurethane Polymer Electrolyte for Solid-State Dye-Sensitized Solar Cell *Jurnal Kejuruteraan* SI1 (3) 2018: pp. 63 – 68. https://doi.org/10.17576/jkukm-2018-si1(3)-09
5. **Adam, N.I., Hanibah, H., Subban, R.H.Y., Kassim, M., Mobarak, N.N., Ahmad, A., Badri, K.H., Su'ait, M.S.** Palm-Based Cationic Polyurethane Membranes for Solid Polymer Electrolytes Application: A Physico-Chemical Characteristics Studies of Chain-Extended Cationic Polyurethane *Industrial Crops and Products* 155 2020: pp. 112757. https://doi.org/10.1016/j.indcrop.2020.112757
6. **Wong, C.S., Badri, K.H., Ataollahi, N., Law, K.P., Su'ait, M.S., Hassan, N.I.** Synthesis of New Bio-Based Solid Polymer Electrolyte Effect of NCO / OH Ratio on Their Chemical, Thermal Properties and Ionic Conductivity *International Journal of Chemical and Molecular Engineering* 8 (11) 2014: pp. 1234 – 1250. https://doi.org/10.5281/zenodo.1096839
7. **Wang, S., Min, K.** Solid Polymer Electrolytes of Blends of Polyurethane and Polyether Modified Polysiloxane and Their Ionic Conductivity *Polymer* 51 (12) 2010: pp. 2621 – 2628.
8. **Jiang, L., Ren, Z., Zhao, W., Liu, W., Liu, H., Zhu, C.** Synthesis and Structure/Properties Characterizations of Four Polyurethane Model Hard Segments *Royal Society Open Science* 5 (7) 2018: pp. 1 – 11. http://dx.doi.org/10.1016/j.polymer.2010.04.038
9. **Filip, D., Asandulesa, M., Macocinschi, D., Aflori, M., Vlad, S.** Molecular Dynamics, Conductivity and Morphology of Sodium Deoxycholate-Based Poly(Ester Ether)Urethane Ionomer Biomaterials *Journal of Materials Science* 51 (18) 2016: pp. 8516 – 8528.
10. **Sharmin, E., Zafar, F.** Polyurethane: An Introduction. Polyurethane. 2012: pp. 3 – 16.
11. **Yeoh, F.H., Lee, C.S., Kang, Y.B., Wong, S.F., Cheng, S.F., Ng, W.S.** Production of Biodegradable Palm Oil-Based Polyurethane as Potential Biomaterial for Biomedical Applications *Polymers* 12 (8) 2020: pp. 1 – 26. https://doi.org/10.3390/polym12081842
12. **Chandima Chathuranga Somarathna, H.M., Raman, S.N., Badri, K.H., Mutalib, A.A., Mohotti, D., Ravana, S.D.** Quasi-static Behavior of Palm-Based Elastomeric Polyurethane: For Strengthening Application of Structures under Impulsive Loadings *Polymers* 8 (5) 2016: pp. 1 – 20. https://doi.org/10.3390/polym8050202
13. **Dian, N.L.H.M., Hamid, R.A., Kanagaratnam, S., Isa, W.R.A., Hassim, N.A.M., Ismail, N.H., Omar, Z., Sahri, M.M.** Palm Oil and Palm Kernel Oil: Versatile Ingredients for Food Applications *Journal of Oil Palm Research* 29 (4) 2017: pp. 487 – 511. http://dx.doi.org/10.21894/jopr.2017.00014
14. **Moreno, D., Velasco, M., Malagón-Romero, D.** Production of Polyurethanes from Used Vegetable Oil-Based Polyols *Chemical Engineering Transaction* 79 2020: pp. 337 – 342. https://doi.org/10.3303/CET2079057
15. **Nainggolan, M., Sinaga, A.** Characteristics of Fatty Acid Composition and Minor Constituents of Red Palm Olein and Palm Kernel Oil *Journal of Advanced Pharmaceutical Technology and Research* 12 (1) 2021: pp. 22 – 26. https://dx.doi.org/10.4103%2Fjaptr.JAPTR_91_20
16. **Sien, W.C., Badri, K.H.** Sifat Terma Dan Kerintangan Api Poliuretana Berasaskan Minyak Isirung Sawit Dan Minyak Kacang Soya *Sains Malaysiana* 39 (5) 2010: pp. 775 – 784.
17. **Arya, A., Sharma, A.L.** Polymer Electrolytes for Lithium Ion Batteries: A Critical Study *Ionics* 23 2017: pp. 497 – 540. https://doi.org/10.1007/s11581-016-1908-6
18. **Löwe, R., Hanemann, T., Zinkevich, T., Hofmann, A.** Structure–Property Relationship of Polymerized Ionic Liquids for Solid-State Electrolyte Membranes *Polymers* 13 (5) 2021: pp. 1 – 12. https://doi.org/10.3390/polym13050792
19. **Somarathna, H.M.C.C., Raman, S.N., Mohotti, D., Mutalib, A.A., Badri, K.H.** Behaviour of Concrete Specimens Retrofitted with Bio-Based Polyurethane Coatings under Dynamic Loads *Construction Building Materials* 270 2021: pp. 121860. https://doi.org/10.1016/j.conbuildmat.2020.121860
20. **Fawzi, T., Yu, L.J., Badri, K.H., Sajuri, Z., Al-Talib, A.A.M., Eh Noum, S.Y.** Sodium Hydrogen Bicarbonate and Water as Blowing Agent in Palm Kernel Oil Based Polyol Polyurethane Foam *Materials Today: Proceedings* 39 2019: pp. 993 – 998. https://doi.org/10.1016/j.matpr.2020.04.595
21. **Awazhar, N.A., Khairuddin, F.H., Rahmad, S., Fadzil, S.M., Omar, H.A., Nur, N.I., Badri, K.H.** Engineering and Leaching Properties of Asphalt Binders Modified with Polyurethane and Cecabase Additives For Warm-Mix Asphalt Application *Construction and Building Materials* 238 2020: pp. 117699. https://doi.org/10.1016/j.conbuildmat.2019.117699

22. **Alamawi, M.Y., Khairuddin, F.H., Yusoff, N.I.M., Badri, K.H., Ceylan, H.** Investigation on Physical, Thermal and Chemical Properties of Palm Kernel Oil Polyol Bio-Based Binder as a Replacement For Bituminous Binder *Construction and Building Materials* 204 2019: pp. 122 – 131. https://doi.org/10.1016/j.conbuildmat.2019.01.144

23. **Jasmi, F., Azeman, N.H., Bakar, A.A.A., Zan, M.S.D., Badri, K.H., Su'ait, M.S.** Ionic Conductive Polyurethane-Graphene Nanocomposite for Performance Enhancement of Optical Fiber Bragg Grating Temperature Sensor *IEEE Access* 6 (i) 2018: pp. 47355 – 47363. https://doi.org/10.1109/ACCESS.2018.2867220

24. **Badri, K.H., Othman, Z., Bin Razali, I.M.** Mechanical Properties of Poyurethane Composites from Oil Palm Resources *Iran Polymer Journal* 14 (5) 2005: pp. 441 – 448.

25. **Badri, K.H.** Biobased Polyurethane from Palm Kernel Oil-Based Polyol. In: Sharmin E, Zafar F. (Eds.) *Polyurethane* 2012: pp. 447 – 470. https://doi.org/10.5772/47966

26. **Ngah, M.S., Badri, K.H.** Pilot Scale System for The Production of Palm-Based Monoester-OH *AIP Conference Proceedings* 2016: pp. 1784. https://doi.org/10.1063/1.4966765

27. **Badri, K.H., Ahmad, S.H., Zakaria, S.** Development of Zero ODP Rigid Polyurethane Foam from RBD Palm Kernel Oil *Journal of Materials Science Letters* 19 (15) 2000: pp. 1355 – 1356. http://dx.doi.org/10.1023/A:1006749131637

28. **Daud, F.N., Ahmad, A., Badri, K.H.** An Investigation on The Properties of Palm-Based Polyurethane Solid Polymer Electrolyte *International Journal of Polymer Science* 2014 2014: pp 1 – 4. https://doi.org/10.1155/2014/326716

29. **Abate, A., Correa-Baena, J.P., Saliba, M., Su'ait, M.S., Bella, F.** Perovskite Solar Cells: From the Laboratory to the Assembly Line *Chemistry – A European Journal* 24 (13) 2018: pp. 3083 – 3100. http://dx.doi.org/10.1002/chem.201704507

30. **Walker, F.,H.** Fundamentals of Polymer Chemistry: II *Journal of Coatings Technology* 73 (913) 2001: pp. 125 – 130.

31. **Gilbert, R.G., Hess, M., Jenkins, A.D., Jones, R.G., Kratochvíl, P., Stepto, R.F.T.** Dispersity in Polymer Science (IUPAC recommendations 2009) *Pure Applied Chemistry* 81 (2) 2009: pp. 351 – 353.

32. **Salleh, M.Z., Badri, K.H., Mahmood, M.H.** Synthesis of UV-Curable Hyperbranched Urethane Acrylate from Palm Oil Oleic Acid *International Journal of Materials Engineering Innovation* 4 (1) 2013: pp. 65 – 78.

33. **Yang, Z., Peng, H., Wang, W., Liu, T.** Morphological, Infrared, and Ionic Conductivity Studies of Poly(ethylene oxide)–49% Poly(methyl methacrylate) Grafted Natural Rubber–Lithium Perchlorate Salt Based Solid Polymer Electrolytes *Journal Applied Polymer Science* 116 (5) 2010: pp. 2658 – 2667. https://doi.org/10.1007/s10008-011-1637-8

34. **Chang, S.C., Yang, Y., Wudl, F., He, G., Li, Y.** Ac Impedance Characteristics and Modeling of Polymer Solution Light-Emitting Devices *Journal of Physical Chemistry B* 105 (46) 2001: pp. 11419 – 11423. https://doi.org/10.1021/jp011817x

35. **Wong, C.S., Badri, K.H.** Chemical Analyses of Palm Kernel Oil-Based Polyurethane Prepolymer *Materials Sciences and Applications* 03 (02) 2012: pp. 78 – 86. http://dx.doi.org/10.4236/msa.2012.32012

36. **Bos, T.** Prediction of Coating Durability – Early Detection using Electrochemical Methods 2008: pp. 148.

37. **Kalsi, P.S.** Spectroscopy of Organic Compounds. 6th Ed. New Dehli: *New Age International Pub.;* 2007.

38. **Orgilés-Calpena, E., Arán-Aís, F., Torró-Palau, A.M., Orgilés-Barceló, C.** Influence of the Chain Extender Nature on Adhesives Properties of Polyurethane Dispersions *Journal of Dispersion Science and Technology* 33 (1) 2012: pp. 147 – 154. https://doi.org/10.1080/01932691.2010.548250

39. **Kurimoto, Y., Takeda, M., Doi, S., Tamura, Y., Ono, H.** Network structures and Thermal Properties of Polyurethane Films Prepared from Liquefied Wood *Bioresour Technology* 77 (1) 2001: pp. 33 – 40. https://doi.org/10.1016/S0960-8524(00)00136-X

40. **Sanchez-Adsuar, M.S., Papon, E., Villenave, J.J.** Influence of the Prepolymerization on the Properties of Thermoplastic Polyurethane Elastomers. Part II. Relationship between the Prepolymer and Polyurethane Properties *Journal of Applied Polymer Science* 76 (10) 2000: pp. 1602 – 1607. http://dx.doi.org/10.1002/(SICI)1097-4628(20000606)76:10<1602::AID-APP16>3.0.CO;2-K

41. **Corcuera, M.A., Rueda, L., Saralegui, A., Martı´n, M.D., Ferna´ndez-d'Arlas, B., Mondragon, I., Eceiza, A.** Effect of Diisocyanate Structure on the Properties and Microstructure of Polyurethanes Based on Polyols Derived from Renewable Resources *Journal of Applied Polymer Science* 122 2011: pp. 3677 – 3685. https://doi.org/10.1002/app.34781

42. **Chattopadhyay, D.K., Webster, D.C.** Thermal Stability and Flame Retardancy of Polyurethanes Progress *Polymer Science (Oxford)* 34 (10) 2009: pp. 1068 – 1133. https://doi.org/10.1016/j.progpolymsci.2009.06.002

43. **Apukhtina, N.P.** Methods for Increasing the Thermal Stability of Polyurethanes *Technomic Pub. Co* 1973.

44. **Lu, M.G., Lee, J.Y., Shim, M.J., Kim, S.W.** Thermal Degradation of Film Cast from Aqueous Polyurethane Dispersions *Journal of Applied Physical Science* 85 (12) 2002: pp. 2552 – 2558. https://doi.org/10.1002/app.10882

45. **Liu, J., Dezhu, M.** Study on Synthesis and Thermal Properties of Polyurethane-Imide Copolymers with Multiple Hard Segments *Journal of Applied Physical Science* 84 (12) 2002: pp. 2206 – 2215. http://dx.doi.org/10.1002/app.10421

46. **Pan, X., Webster, D.C.** New Biobased High Functionality Polyols and Their Use in Polyurethane Coatings *ChemSusChem* 5 (2) 2012: pp. 419 – 429. https://doi.org/10.1002/cssc.201100415

47. **Rueda-Larraz, L., d'Arlas, B.F., Tercjak, A., Ribes, A., Mondragon, I., Eceiza, A.** Synthesis and Microstructure-Mechanical Property Relationships of Segmented Polyurethanes based on a PCL-PTHF-PCL Block Copolymer As Soft Segment *European Polymer Journal* 45 (7) 2009: pp. 2096 – 2109. https://doi.org/10.1002/cssc.201100415

48. **Retter, U., Widmann, A., Siegler, K., Kahlert, H.** On The Impedance of Potassium Nickel(II) Hexacyanoferrate(II) Composite Electrodes – The Generalization of the Randles Model Referring To Inhomogeneous Electrode Materials *Journal Electroanal Chemistry* 546 2003: pp. 87 – 96. http://dx.doi.org/10.1016/S0022-0728(03)00150-5

49. **Potamianou, S.F., Thoma, K.A.T., Pisanias, M.N.** A Study on a Numerical Solution of The Transport Equations for Thin Insulating Films with Two Blocking Electrodes *Journal of Physics A: Mathematical and General* 23 (7) 1990: pp. 1313 – 1321. https://doi.org/10.1088/0305-4470/23/7/033

50. **Bayrak, R., Dumludağ, F., Akçay, H.T., Değirmencioğlu, I.** Synthesis, Characterization and Electrical Properties of Peripherally Tetra-Aldazine Substituted Novel Metal Free Phthalocyanine and its Zinc(II) and Nickel(II) Complexes *Spectrochimica Acta – Part A: Molecular and Biomolecular Spectroscopy* 105 2013: pp. 550 – 556. https://doi.org/10.1016/j.saa.2012.12.058

51. **Skoog, D.A., Holler, F.J.C.S.** Principles of Instrumental Analysis. Cengage Learning, 2007: pp. 9.

52. **Carpi, F., De Rossi, D.** Electroactive Polymer Artificial Muscles: An Overview *WIT Transactions on Ecology and the Environment* 138 2010: pp. 353 – 364. https://doi.org/10.2495/DN100311

53. **Su'ait, M.S., Ahmad, A., Badri, K.H., Mohamed, N.S., Rahman, M.Y.A., Ricardo, C.L.A., Scardi, P.** The Potential of Polyurethane Bio-Based Solid Polymer Electrolyte for Photoelectrochemical Cell Application *International Journal of Hydrogen Energy* 39 (6) 2014: pp. 3005 – 3017. https://doi.org/10.1016/j.ijhydene.2013.08.117

54. **Su'ait, M.S., Ahmad, A., Hamzah, H., Rahman, M.Y.A.** Effect of Lithium Salt Concentrations on Blended 49% Poly(Methyl Methacrylate) Grafted Natural Rubber and Poly(Methyl Methacrylate) based Solid Polymer Electrolyte *Electrochimica Acta* 57 (1) 2011: pp. 123 – 131. https://doi.org/10.1016/j.electacta.2011.06.015